

## Effects of shock waves on Rayleigh-Taylor instability

Yong-Tao Zhang<sup>a)</sup>

*Department of Mathematics, University of California at Irvine, Irvine, California 92697*

Chi-Wang Shu<sup>b)</sup>

*Division of Applied Mathematics, Brown University, Providence, Rhode Island 02912*

Ye Zhou<sup>c)</sup>

*Lawrence Livermore National Laboratory, University of California, Livermore, California 94550*

(Received 25 October 2005; accepted 29 March 2006; published online 14 June 2006)

A numerical simulation of two-dimensional compressible Navier-Stokes equations using a high-order weighted essentially nonoscillatory finite difference shock capturing scheme is carried out in this paper, to study the effect of shock waves on the development of Rayleigh-Taylor instability. Shocks with different Mach numbers are introduced ahead or behind the Rayleigh-Taylor interface, and their effect on the transition to instability is demonstrated and compared. It is observed that shock waves can speed up the transition to instability for the Rayleigh-Taylor interface significantly. Stronger shocks are more effective in this speed-up process. © 2006 American Institute of Physics. [DOI: 10.1063/1.2201063]

### I. INTRODUCTION

In this paper, we are interested in studying the effect of shock waves on the development of Rayleigh-Taylor instability (RTI), through a numerical simulation of the two-dimensional Navier-Stokes equations using a high-order weighted essentially nonoscillatory (WENO) finite difference shock capturing scheme.

Rayleigh-Taylor instability results from the application of a pressure gradient (e.g., a gradient due to gravity) in the direction opposite to a density gradient.<sup>1-4</sup> It happens on an interface between fluids with different densities when an acceleration is directed from the heavy fluid to the light fluid. The instability has a fingering nature, with bubbles of light fluid rising into the ambient heavy fluid and spikes of heavy fluid falling into the light fluid; see, for example, Refs. 5 and 6. Eventually, a flow induced by RTI will develop into a high Reynolds number turbulence with very strong nonlinearity.<sup>7</sup> The turbulent flows induced by RTI have found a wide range of applications both in an astrophysical setting<sup>8,9</sup> and in an inertial confinement fusion.<sup>10</sup> Progress in an understanding of RTI-induced flows<sup>11</sup> will hopefully lead to improved models for astrophysical and engineering calculations.<sup>12,13</sup>

When an external agency is present, the evolution of an RTI-induced flow will be significantly modified. Carnevale *et al.*<sup>14</sup> demonstrated that the growth of the mixing zone generated by RTI can be greatly retarded by the application of rotation. Specifically, for a weak rotation, the development of the mixing zone would not proceed as far as that of a non-rotating case. For a strong rotation, however, the growth of the perturbation would be diminished so significantly that there is little that can be identified as a mixing layer formation. Pacitto *et al.*<sup>15</sup> reported an RTI experiment using a

magnetic fluid and applying a magnetic field. These authors measured different values of the magnetic field, the wavelength, and the growth rate of the observed pattern. The magnetic field was found to destabilize the interface, decrease the wavelength, and increase the growth rate.

The important work by Mügler and Gauthier<sup>16</sup> provided a comprehensive study of a Richtmyer-Meshkov (RM) flow subject to reshock. They used both carefully controlled experiments and numerical simulations. The initial mixing layer was induced by an RM instability. These authors found that the reshock accelerated the transition to turbulence process. Our initial mixing layer, however, was induced by a Rayleigh-Taylor (RT) instability. We are interested in how a mixing layer induced by an RT instability interacts with shock waves. Despite many similarities, a mixing layer induced by an RT instability is different from that which would result from an RM instability. Therefore, it is important to differentiate the work between Mügler and Gauthier<sup>16</sup> from that of our present paper.

Another major difference between our work and that of Mügler and Gauthier<sup>16</sup> is the range of Mach numbers of the flow under consideration. The RM reshock experiments are usually restricted to relatively low Mach number regime. However, in our numerical simulations, we have investigated the interactions between the RT-induced mixing layer and shock waves of a wide range of values in Mach number.

In summary, the objective of this paper is to study the effect of shock waves on the development of the Rayleigh-Taylor instability. Shocks with different Mach numbers are introduced ahead or behind the Rayleigh-Taylor interface, and their effect on the transition to instability is demonstrated and compared. It is observed that shock waves can speed up the transition to instability for the Rayleigh-Taylor interface significantly. Stronger shocks are more effective in this speed-up process.

<sup>a)</sup>Electronic mail: zyt@math.uci.edu

<sup>b)</sup>Electronic mail: shu@dam.brown.edu

<sup>c)</sup>Electronic mail: zhou3@llnl.gov

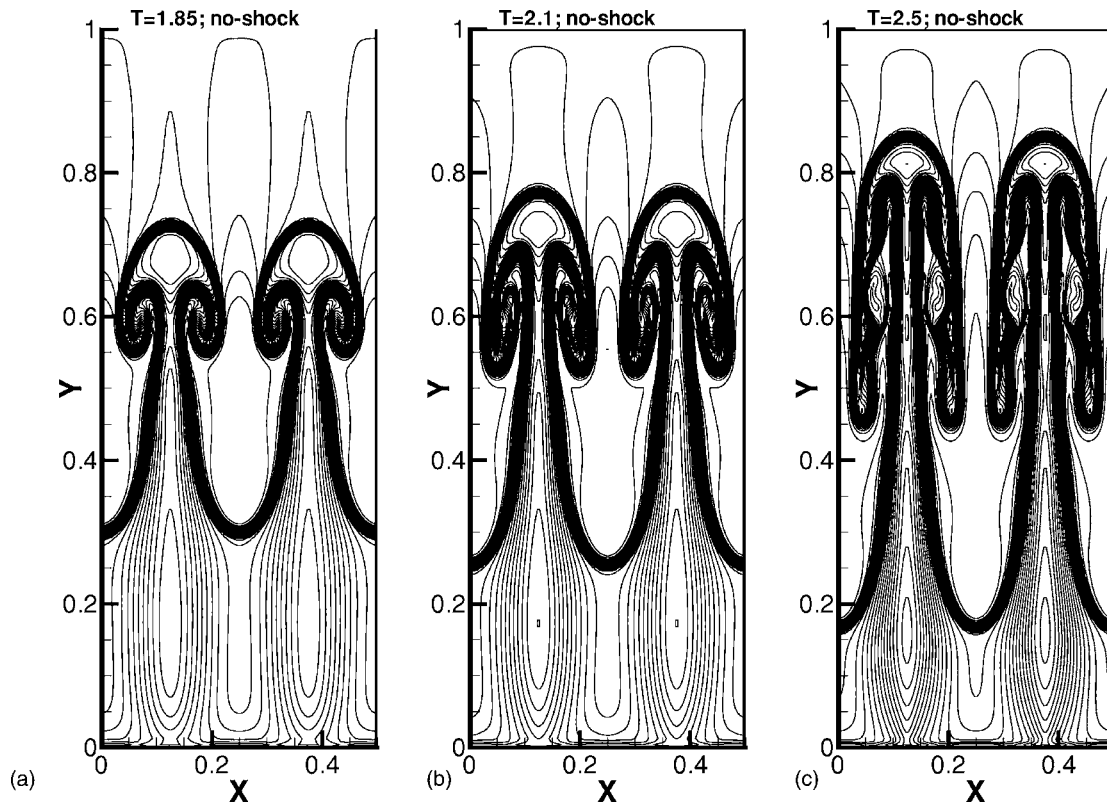


FIG. 1. Rayleigh-Taylor flow at different time. (a)  $T=1.85$ ; (b)  $T=2.1$ ; (c)  $T=2.5$ . Density  $\rho$ ; 45 equally spaced contour lines.

## II. NUMERICAL METHOD AND RTI SETUP

Numerical experiments are performed using a ninth-order finite difference WENO scheme<sup>17</sup> associated with an eighth-order central approximation to the viscous terms, for the two-dimensional nondimensionalized Navier-Stokes equations with gravitation source terms,

$$\rho_t + (\rho u)_x + (\rho v)_y = 0,$$

$$(\rho u)_t + (\rho u^2 + p)_x + (\rho uv)_y = \frac{1}{\text{Re}} \left( \frac{4}{3} u_{xx} + u_{yy} + \frac{1}{3} v_{xy} \right), \quad (1)$$

$$(\rho v)_t + (\rho uv)_x + (\rho v^2 + p)_y = \frac{1}{\text{Re}} \left( v_{xx} + \frac{4}{3} v_{yy} + \frac{1}{3} u_{xy} \right) + \rho,$$

$$\begin{aligned} E_t + [u(E+p)]_x + [v(E+p)]_y \\ = \frac{1}{\text{Re}} \left( \frac{2}{3} (u^2)_{xx} - \frac{2}{3} (uv)_x + \frac{1}{2} (v^2)_{xx} \right. \\ \left. + (vu_y)_x + \frac{1}{2} (u^2)_{yy} + (uv_x)_y + \frac{2}{3} (v^2)_{yy} - \frac{2}{3} (vu_x)_y \right) \\ \left. + \frac{1}{(\gamma-1)\text{Pr}} [(C^2)_{xx} + (C^2)_{yy}] + \rho v, \right. \end{aligned}$$

where  $\rho$  is the density,  $(u, v)$  is the velocity,  $E$  is the total energy, and  $p$  is the pressure, related to the total energy by  $E = p/(\gamma-1) + \frac{1}{2}\rho(u^2+v^2)$  with the ratio of specific heats  $\gamma$  being a constant.  $C$  is the sound speed satisfying  $C^2 = \gamma p/\rho$ ,  $\text{Re}$  is the Reynolds number,  $\text{Pr}=0.7$  is the Prandtl number.

The class of high-order finite difference WENO schemes, coupled with total variation diminishing (TVD) high-order Runge-Kutta time discretizations,<sup>18</sup> was developed in Ref. 19 for the fifth-order accurate version and in Ref. 17 for the higher-order versions, including the ninth-order version that we use in this paper. The resolution of these high-order WENO schemes when applied to high Reynolds number Navier-Stokes equations has been studied in detail in Ref. 20. It was shown in Ref. 20 that it is advantageous in terms of CPU time to use a higher-order WENO scheme to simulate flows with both shocks and complicated smooth flow features, such as the problem of Rayleigh-Taylor instability under study. This is the motivation for us to choose the ninth-order WENO scheme<sup>17</sup> for the simulation in this paper. The Reynolds number in the Navier-Stokes equations (1) is taken as  $\text{Re}=25\,000$ , which requires a mesh size  $h=1/240$  in order to obtain resolved numerical solutions according to the study in Ref. 20.

We set up the RTI as follows. The computational domain is  $[0, \frac{1}{2}] \times [0, 1]$ . Initially the interface is at  $y = \frac{1}{2}$ . The heavy fluid with density  $\rho=2$  is below the interface, and the light fluid with density  $\rho=1$  is above the interface with the acceleration in the positive  $y$  direction. The pressure  $p$  is continuous across the interface. A small perturbation is given to the  $y$ -direction fluid speed; thus for  $0 \leq y < \frac{1}{2}$ ,  $\rho=2$ ,  $u=0$ ,  $p=2y+1$ ,  $v=-0.025C \cdot \cos(8\pi x)$ , and for  $\frac{1}{2} \leq y \leq 1$ ,  $\rho=1$ ,  $u=0$ ,  $p=y+\frac{3}{2}$ ,  $v=-0.025C \cdot \cos(8\pi x)$ , where  $C$  is the sound speed,  $C = \sqrt{\gamma p/\rho}$ , and the ratio of specific heats  $\gamma = \frac{5}{3}$ . Reflective boundary conditions are imposed for the left and

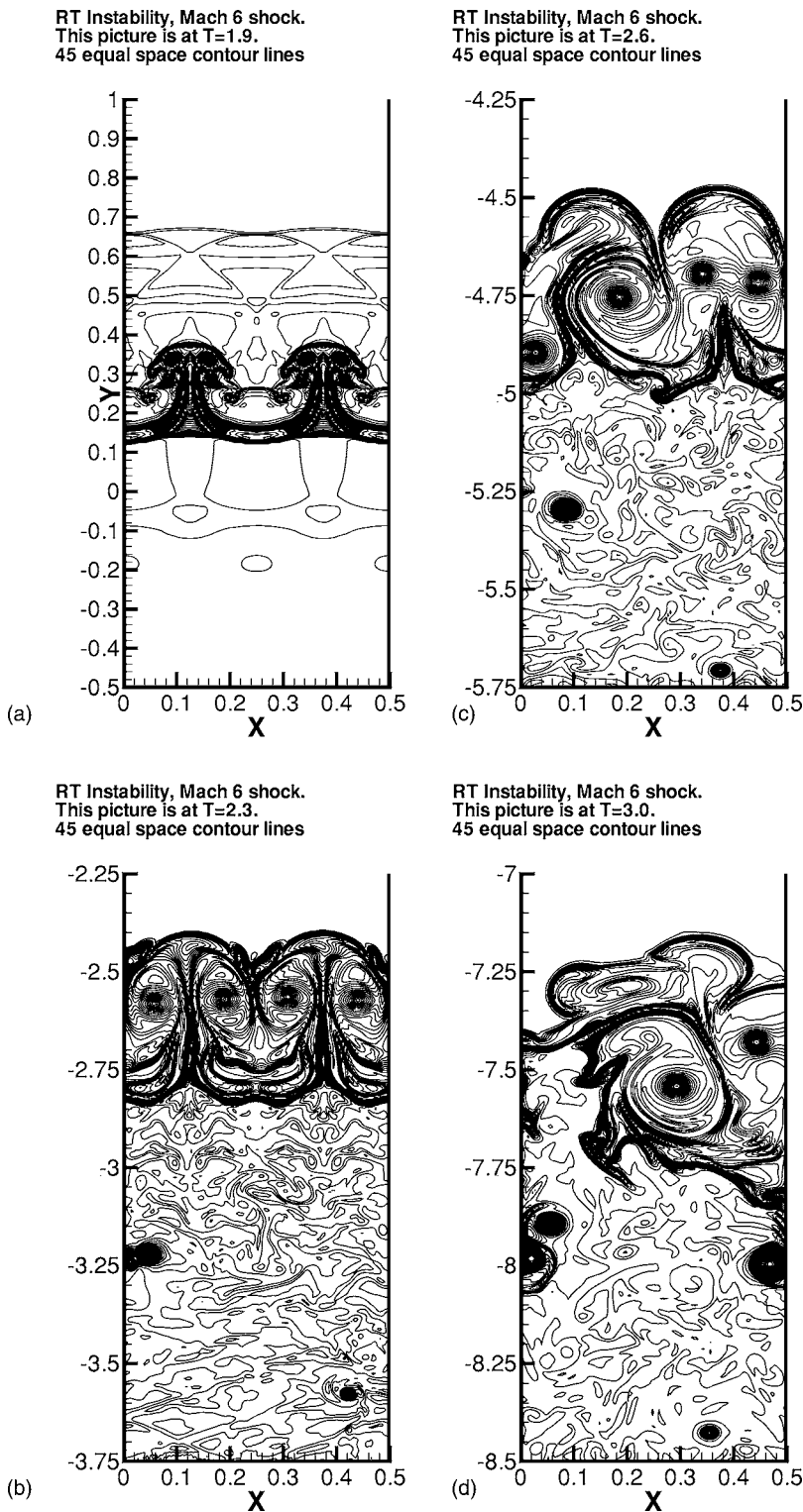


FIG. 2. Mach 6 shock interacting with a Rayleigh-Taylor flow. Shock hits the head of the RT interface at  $T=1.85$ . From left to right, the Rayleigh-Taylor interface at (a)  $T=1.9$ ; (b)  $T=2.3$ ; (c)  $T=2.6$ ; (d)  $T=3.0$ . Density  $\rho$ ; 45 equally spaced contour lines.

right boundaries. At the top boundary, the flow values are set as  $\rho=1$ ,  $p=2.5$ ,  $u=v=0$ , and at the bottom boundary, they are set as  $\rho=2$ ,  $p=1$ ,  $u=v=0$ . Notice that the source term  $\rho$  is added to the right-hand side of the third equation and  $\rho v$  is added to the fourth equation in the Navier-Stokes system (1).

In Fig. 1, the Rayleigh-Taylor flow at  $T=1.85$ , 2.1, and 2.5 is shown. This should serve as a reference to compare with the results in the next section when shock waves are introduced into the flow.

### III. SIMULATED RTI FLOW FIELDS AND SHOCK WAVES

We now introduce shocks with different Mach numbers to hit the Rayleigh-Taylor interface at a fixed time  $T=1.85$ , and observe the effects of shock waves when they interact with the RTI flow.

First we put shock waves with Mach numbers 6, 12, 18, 24 into the computational domain from the top

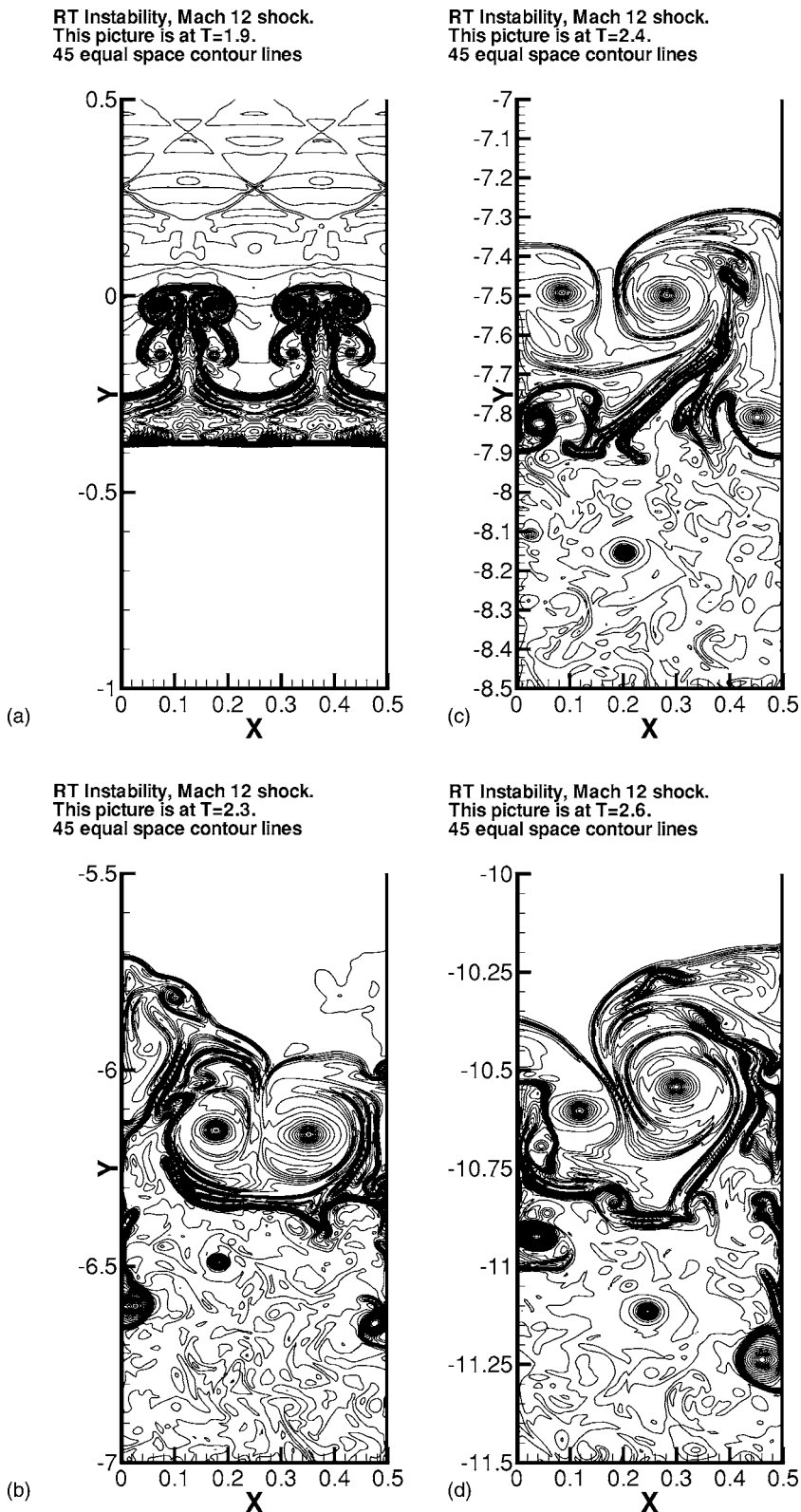


FIG. 3. Mach 12 shock interacting with a Rayleigh-Taylor flow. Shock hits the head of the RT interface at  $T=1.85$ . From left to right, the Rayleigh-Taylor interface at (a)  $T=1.9$ ; (b)  $T=2.3$ ; (c)  $T=2.4$ ; (d)  $T=2.6$ . Density  $\rho$ ; 45 equally spaced contour lines.

boundary at different times, so that different shock waves hit the head of the Rayleigh-Taylor flow at the same time  $T=1.85$ . The unshocked fluid is the top fluid state:  $\rho=1$ ,  $p=2.5$ ,  $u=v=0$ . Since the moving shock wave makes the RT interface move downward, in order to observe the development of the RT interface at a later time, we extend the computational domain in the simulations to avoid the RT inter-

face moving out of the computational domain. For the shock waves hitting the head of the RT interface, we extend the computational domain in the  $y$  direction to  $[-20, 1]$ . The initial condition for the domain  $y < 0$  is the mean flow  $\rho=2$ ,  $p=1$ ,  $u=v=0$ ; the boundary condition at  $y=-20$  is set to be an outflow. Figure 2 shows the Rayleigh-Taylor interface at four different times after a Mach 6 shock wave hits the head

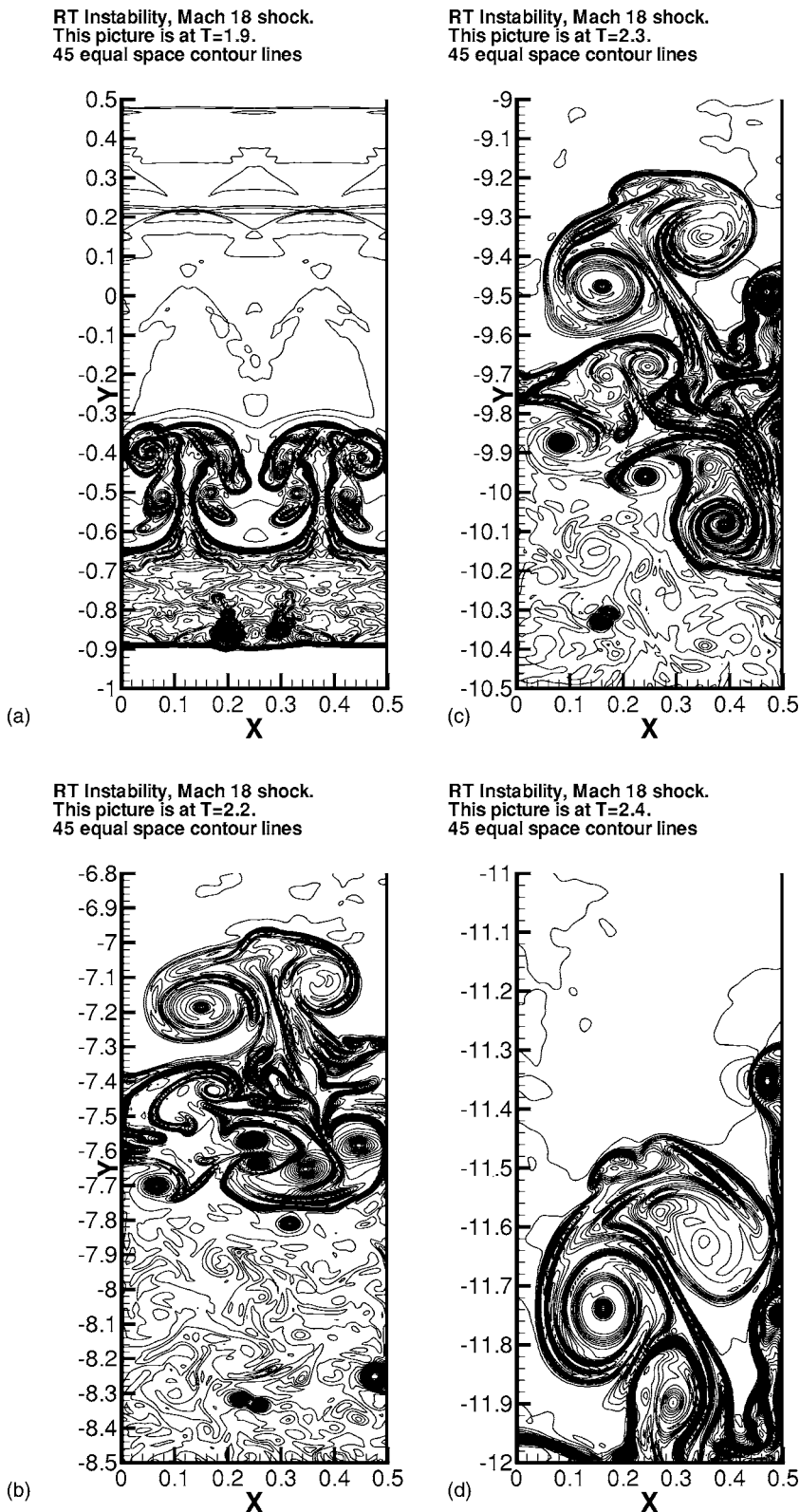


FIG. 4. Mach 18 shock interacting with a Rayleigh-Taylor flow. Shock hits the head of the RT interface at  $T=1.85$ . From left to right, the Rayleigh-Taylor interface at (a)  $T=1.9$ ; (b)  $T=2.2$ ; (c)  $T=2.3$ ; (d)  $T=2.4$ . Density  $\rho$ ; 45 equally spaced contour lines.

of RTI at  $T=1.85$  and passes through the RT interface. Cases for stronger shock waves are presented in Figs. 3–5, for shock Mach numbers 12, 18, and 24, respectively. We observe the effect of strong shock waves speeding up the transition of the RT flow to instability. The stronger the shock wave is, the earlier the RT flow develops into full instability.

The same conclusion is drawn when we put shock wave

into the computational domain from the bottom boundary to hit the tail of the Rayleigh-Taylor interface. The unshocked fluid is the bottom fluid state:  $\rho=2$ ,  $p=1$ ,  $u=v=0$ . Again, since the moving shock waves make the RT interface move upward, in order to observe the development of the RT interface at a later time, the computational domain in the  $y$  direction is extended to  $[0, 20]$ . The initial condition for the

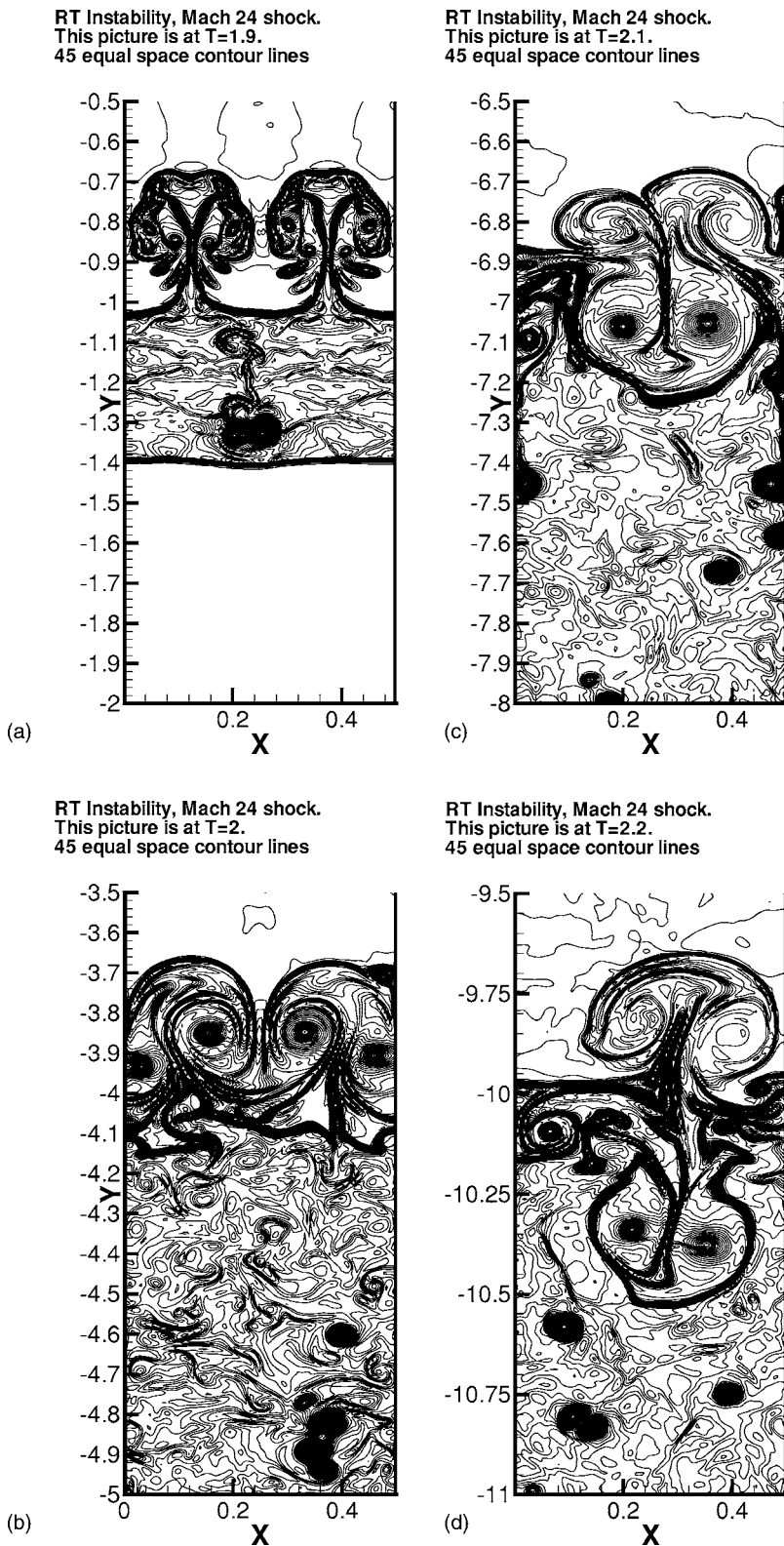


FIG. 5. Mach 24 shock interacting with a Rayleigh-Taylor flow. Shock hits the head of the RT interface at  $T=1.85$ . From left to right, the Rayleigh-Taylor interface at (a)  $T=1.9$ ; (b)  $T=2$ ; (c)  $T=2.1$ ; (d)  $T=2.2$ . Density  $\rho$ ; 45 equally spaced contour lines.

domain  $y > 1$  is the mean flow  $\rho=1$ ,  $p=2.5$ ,  $u=v=0$ ; the boundary condition at  $y=20$  is set to be an outflow. The right picture in Fig. 6 shows the RT interface at  $T=3$  after a Mach 12 shock hits the tail of the RT interface at  $T=1.85$ . Also in Fig. 6, we compare the RT interface at  $T=6$  for the case without shock interaction, and the RTI flow at  $T=3$  for the two cases with shock interaction. The shock Mach number is

12 for both cases of the shock hitting the head and hitting the tail of the RT interface. We can observe that the shock waves do speed up the transition of the RT flow to full instability in each case.

We also present selective results for the temperature, entropy, and vorticity in Figs. 7–10, at the time when the shock just hits the tip of the RT interface and at the time when the

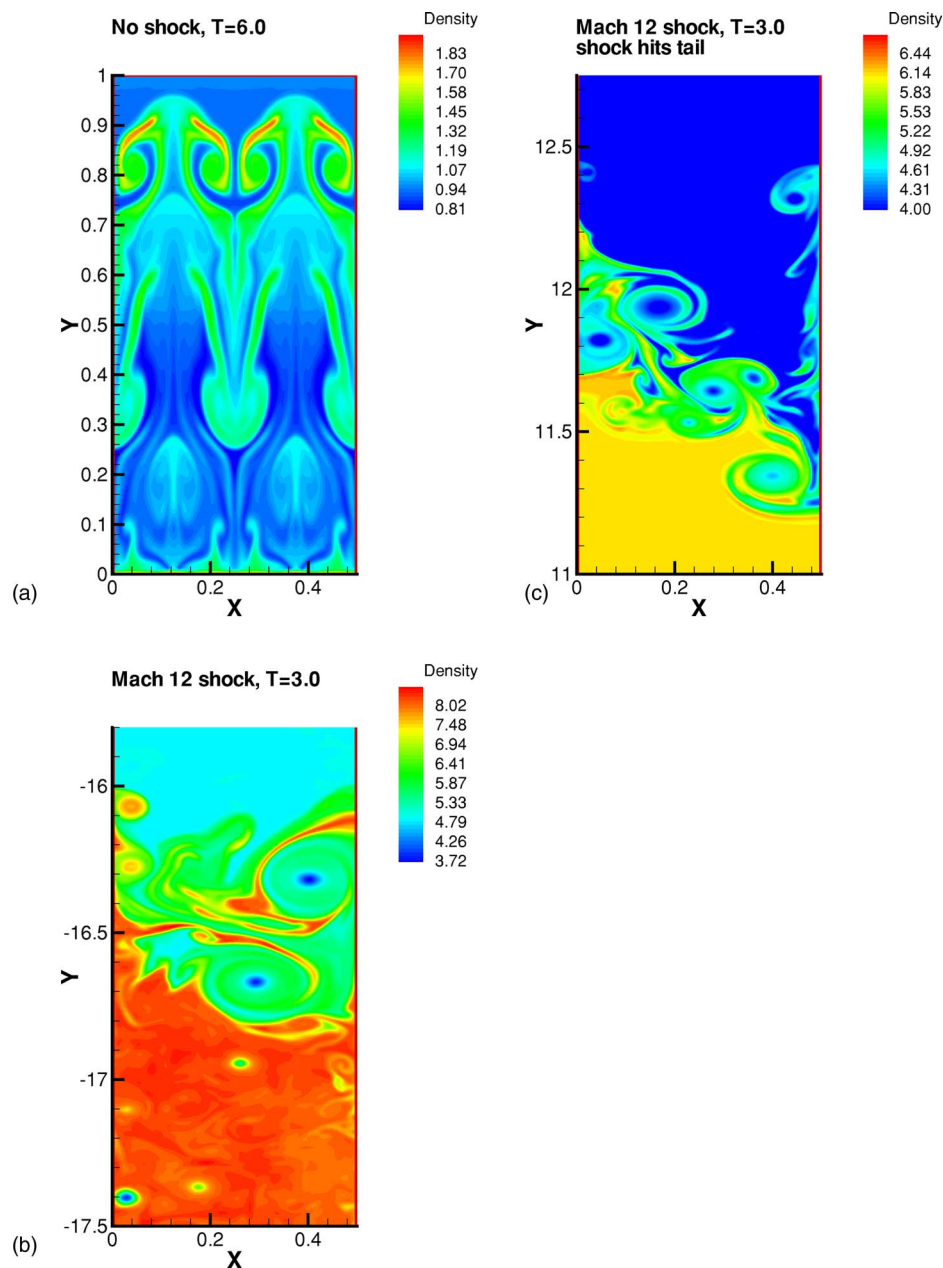


FIG. 6. (Color online) (a) The Rayleigh-Taylor flow at  $T=6.0$ ; (b) Mach 12 shock hitting the Rayleigh-Taylor interface from the top,  $T=3.0$ ; (c) Mach 12 shock hitting the Rayleigh-Taylor interface from the bottom,  $T=3.0$ . The time when shock hits the RT interface is  $T=1.85$  for both cases of the shock coming from the top and from the bottom. Density  $\rho$ .

shock just leaves the tail of the RT interface, respectively, for the Mach 6 and Mach 24 cases. Both color contours and selected one-dimensional cuts are shown to reveal the physical process during this short time period.

We remark that even though the initial condition and algorithm are both symmetric, the computed results lose symmetry when full instability develops, due to round-off errors and their amplification by the physical instability. This is common in RT simulations; see, for example, Ref. 21, where there is a grid refinement study and loss of symmetry appears when the grid is refined enough such that physical instability dominates the flow.

#### IV. INTERACTION OF SHOCK WAVES AND THE RTI

In this section, we make a more detailed inspection on the physical consequences of a shock wave interacting with an evolving RT flow. In particular, we are interested in

whether the shock wave will diminish (as in the case of rotating flow) or enhance (as in the case of magnetic fluid) the growth of the mixing zone. Furthermore, we will investigate how such an effect depends on the strength of the shock.

Figures 2–5 show the time dependence of the RTI flows after being hit by a shock wave at Mach numbers 6, 12, 18, and 24. As the strength of the shock wave increases, the location of the RTI interface moves downward with the shock wave hitting the head of the interface.

We first look at the observation time at  $T=1.9$  in Figs. 2(a), 3(a), 4(a), and 5(a). Recall that the shock hits the evolving RTI flow at  $T=1.85$ , therefore, we are observing in these figures the effects of the shock strength at an early time. We can see a modest positive correlation between the strength of the shock wave and the growth of height and complexity of the structures (with the development of the associated sec-

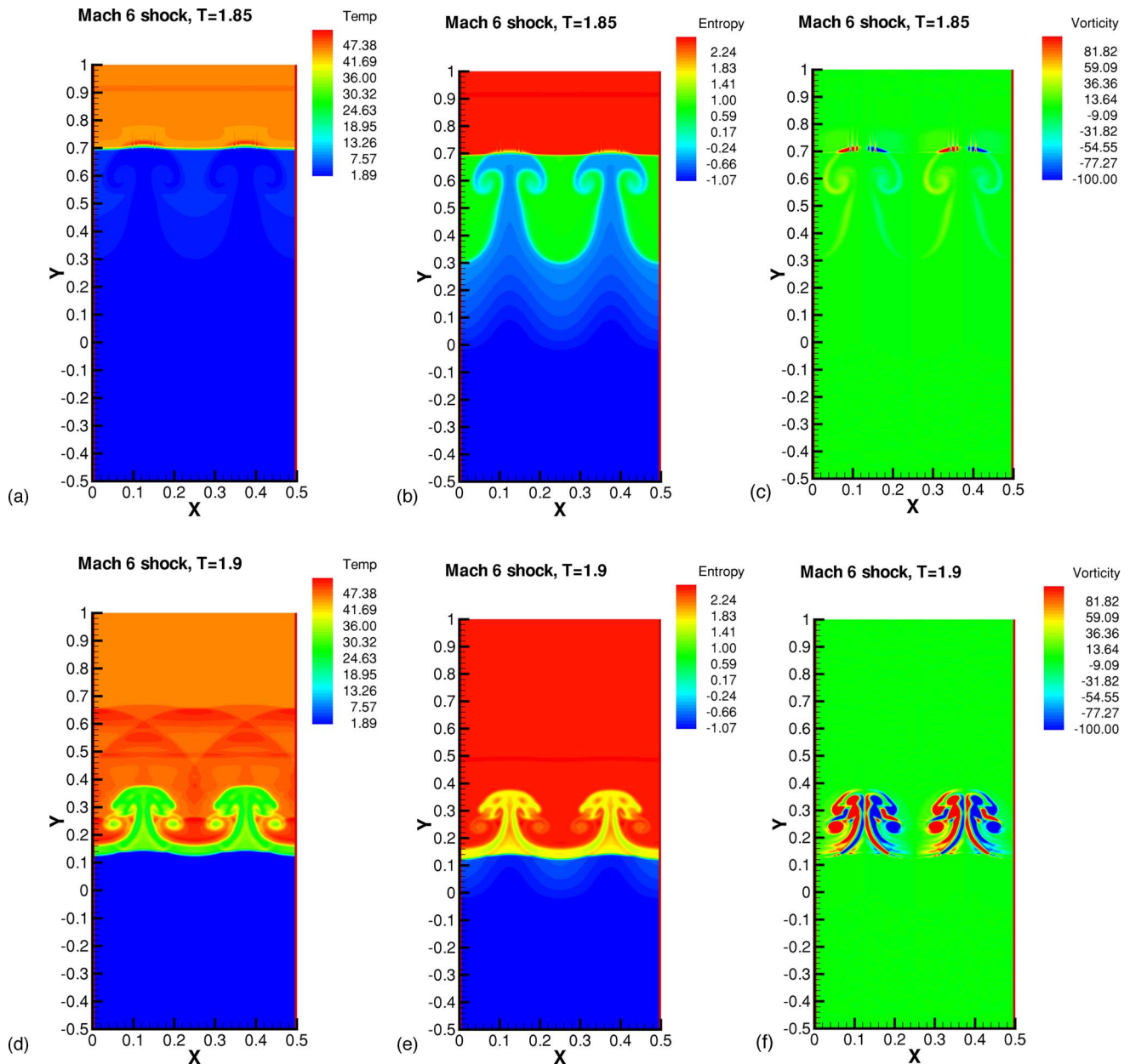


FIG. 7. (Color online) Mach 6 shock interacts with Rayleigh-Taylor flows. Top: shock just hits the head of the RT interface at  $t=1.85$ ; bottom: shock just leaves the tail of the RT interface at  $t=1.9$ . Left: temperature; middle: entropy; right: vorticity.

ondary instability—Kelvin-Helmholtz instability).

We now look at time  $T=2.3$  for Mach 6, 12, and 18 [Figs. 2(b), 3(b), and 4(c)]. It is apparent that a strong shock will speed up the development of the mixing layer. With the Mach 6 shock wave, the two structures are still well organized. However, the symmetry is already lost when the Mach 12 shock is employed. When the Mach number reaches 18, we note that the width of the mixing zone has increased significantly. Also, the two symmetric structures in Fig. 2(b) have already merged into one.

Comparing Figs. 2(c) and 3(d) (Mach 6 and 12 at  $T=2.6$ ), we observe that the two structures are at relatively early and later stages of the merging process, respectively. The similar trend is also observed in Figs. 3(c) and 4(d) (at  $T=2.4$ ). For the case of Mach 12, the structures are in the relatively late stage of the merging, but this process is al-

ready completed when the Mach number is increased to 18.

When the Mach numbers become very high at 18 and 24, we find that the structures of mixing layer are quite similar at  $T=2.2$  [Figs. 4(b) and 5(d)]. We conjecture that after exceeding some large Mach number, the values of this important parameter may become irrelevant to the detailed process of disrupting the development of an RTI flow by a shock wave. Clearly, additional studies are needed.

We also investigate whether the direction of the shock wave has any consequence on the future development of the mixing layer. Figure 6 suggests that there is a difference in the resulting mixing layer.

To gain some insights on how the shock accelerated the transition to the turbulence process, we now turn our attention to the temperature, entropy, and vorticity measurements of the Rayleigh-Taylor flows at Mach number 6 (Fig. 7).

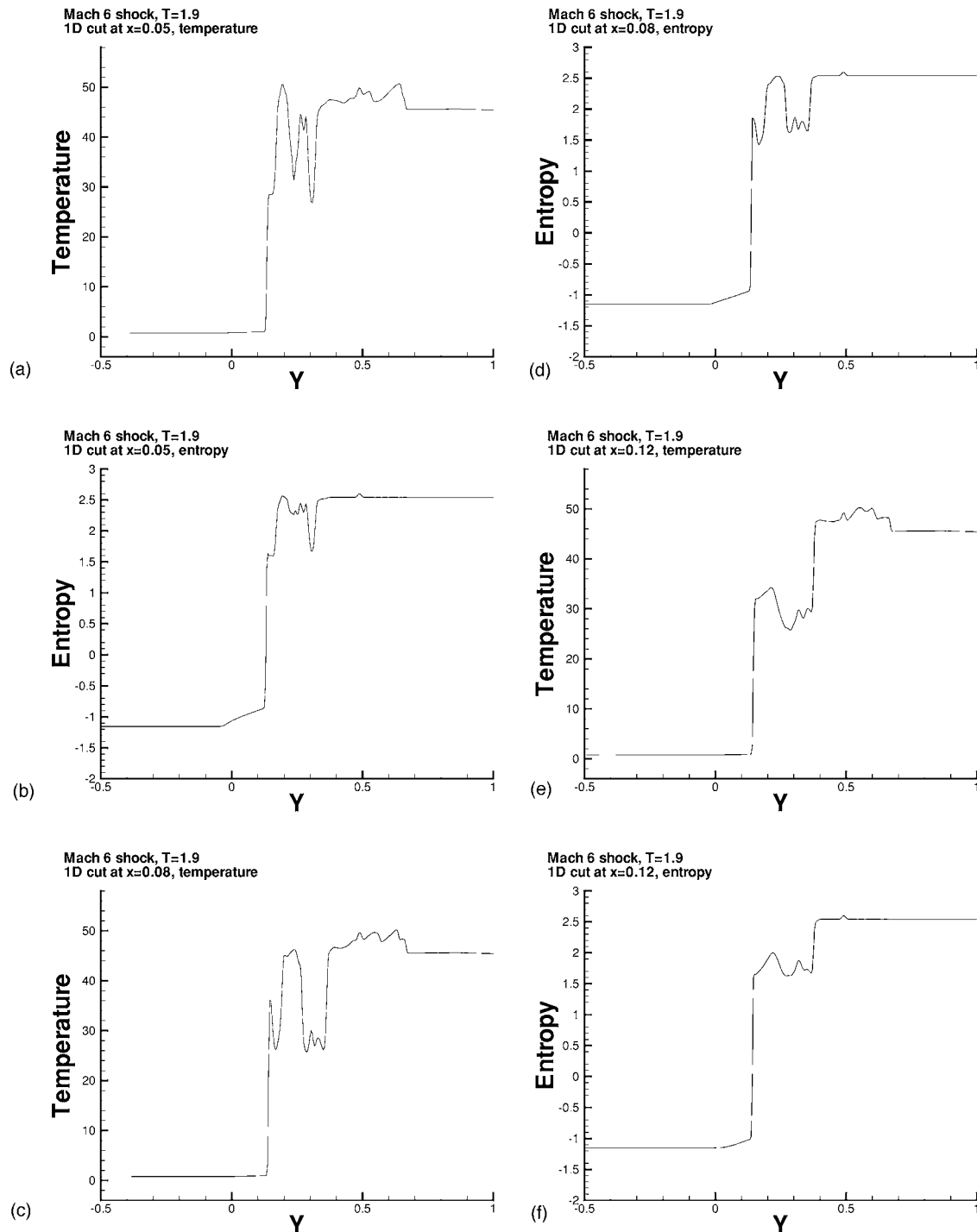


FIG. 8. Mach 6 shock interacts with Rayleigh-Taylor flows. 1D-cut pictures.  $t=1.9$ .

When the shock just hits the head of the interface ( $T=1.85$ ), there is a fairly sharp division for the temperature field along the shock location [Fig. 7(a)]. The mushroom structures generated by the RT instability have not yet changed from their original entropy values [Fig. 7(b)], and the vorticity is relatively small [Fig. 7(c)].

However, immediately after the passage of the shock wave ( $T=1.9$ ), the temperature of the mushroom structures increases rapidly [Fig. 7(d)]. The entropy of the mushroom structures also increases significantly [Fig. 7(e)]. This is consistent with the usual understanding that an energy deposi-

tion will result with a passage of a shock. The vorticity is also significantly enhanced [Fig. 7(f)].

Additional insights can be obtained by taking one-dimensional cuts for the temperature and entropy plots. We only need to consider the situation after the shock passage (Fig. 8) and to focus on one of the two structures because of the symmetry. Three  $x$  locations are considered. It is interesting to observe that the temperature and entropy at the stem of the mushroom ( $x=0.12$ ) are lower than those at the other two locations. This explains why the flow structure is relatively stable at this location. On the other hand, the temperature

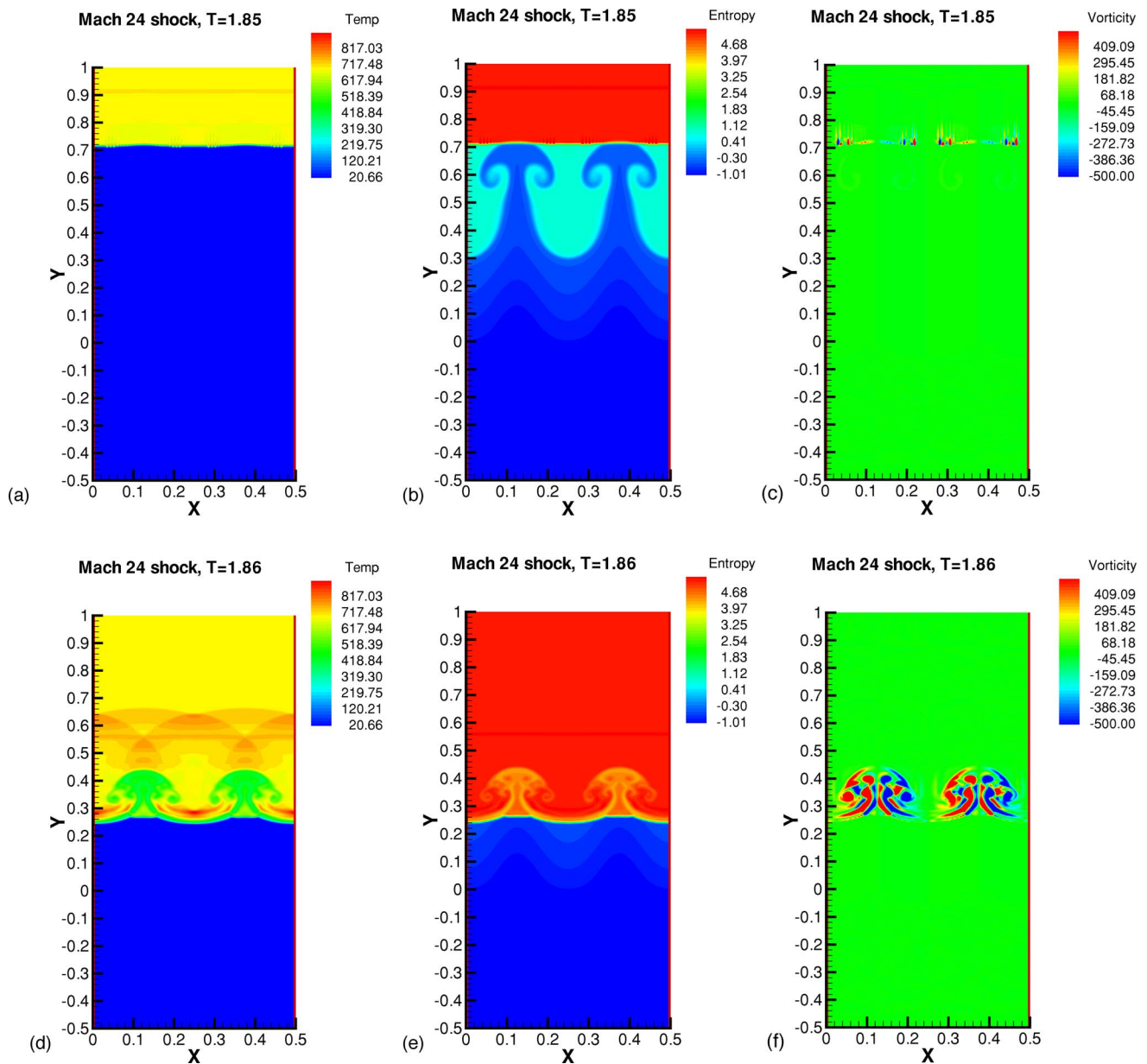


FIG. 9. (Color online) Mach 24 shock interacts with Rayleigh-Taylor flows. Top: shock just hits the head of the RT interface at  $t=1.85$ ; bottom: shock just leaves the tail of the RT interface at  $t=1.86$ . Left: temperature; middle: entropy; right: vorticity.

and entropy measurements at the cap of the mushroom ( $x=0.08$ ) and at a spin off structure ( $x=0.05$ ) are higher. This suggests that these regions have a much higher level of energy. These higher values of temperature and entropy will lead to the breaking down of the flow structures into much smaller ones.

We have also investigated the case of Mach 24 in order to observe the Mach number effect. When the Mach number of the shock is increased, the temperature of the mushroom structures changes to a much higher value [Figs. 9(a) and 9(d), before and after the shock passage]. The entropy gained by the mixing layer is also much higher than that of the Mach 6 case [Figs. 9(b) and 9(e)]. Likewise, the enhancement of vorticity is also more significant [Figs. 9(f) and 9(c)]. These higher-energy depositions at Mach 24 are the major reason why the mixing layer in this case develops

much faster than that of a lower Mach number.

The one-dimensional cuts of both temperature and entropy (Fig. 10) are very similar to that of the Mach 6 case. These results suggest that the physical process of the mixing layer development remains the same, but at a different rate.

Finally, we offer some comments based on vorticity dynamics. Generically, an interface of two fluids with different densities is associated with a weak vortex layer,<sup>22,23</sup> as can be recognized from Fig. 7(c). In Ref. 24 Tryggvason performed a two-dimensional numerical simulation of the Rayleigh-Taylor instability in terms of interfacial vortex sheet dynamics. The shock wave, in our study, becomes curved after hitting the RT structure and results in highly uneven distributions of both the temperature and entropy fields [Figs. 7(d), 7(e), 9(d), and 9(e)]. The baroclinic source of vorticity<sup>25-27</sup> is generated and is responsible for the for-

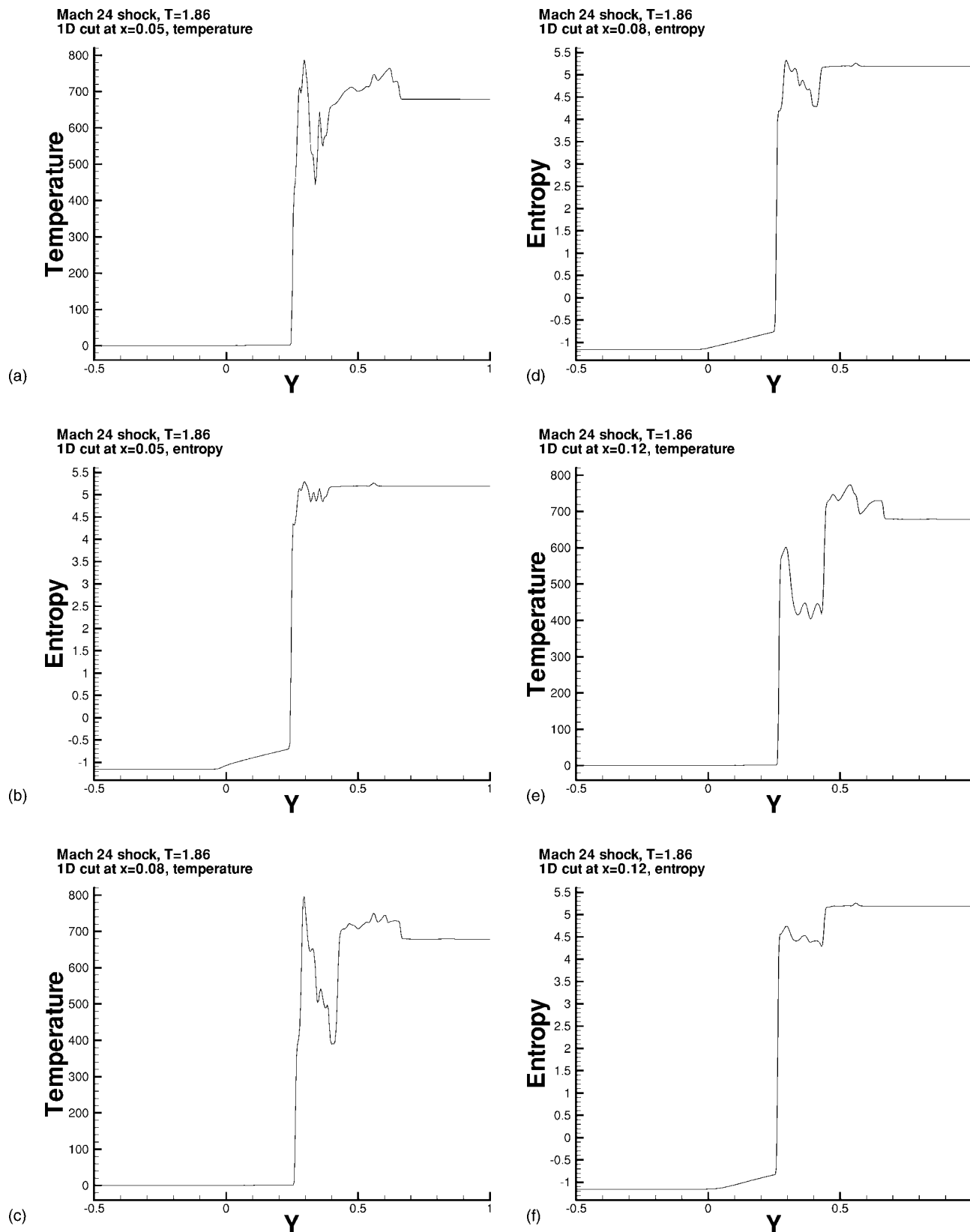


FIG. 10. Mach 24 shock interacts with Rayleigh-Taylor flows. 1D-cut pictures.  $t=1.86$ .

mation of the mushroom-like vortex layers [Figs. 7(f) and 9(f)]. These strong vortex layers and the associated strong dilatation layer will induce a further deformation of the interface via the generalized Biot-Savart law. The  $z$  component of the cross product of temperature gradient and entropy gra-

dient (the baroclinic term) also shows the two-sign vorticity source (Fig. 11). As a result, the passage of a shock accelerates the destruction of the organized RT mushroom-like structure and speeds up the transition of the flow to fully developed turbulence.

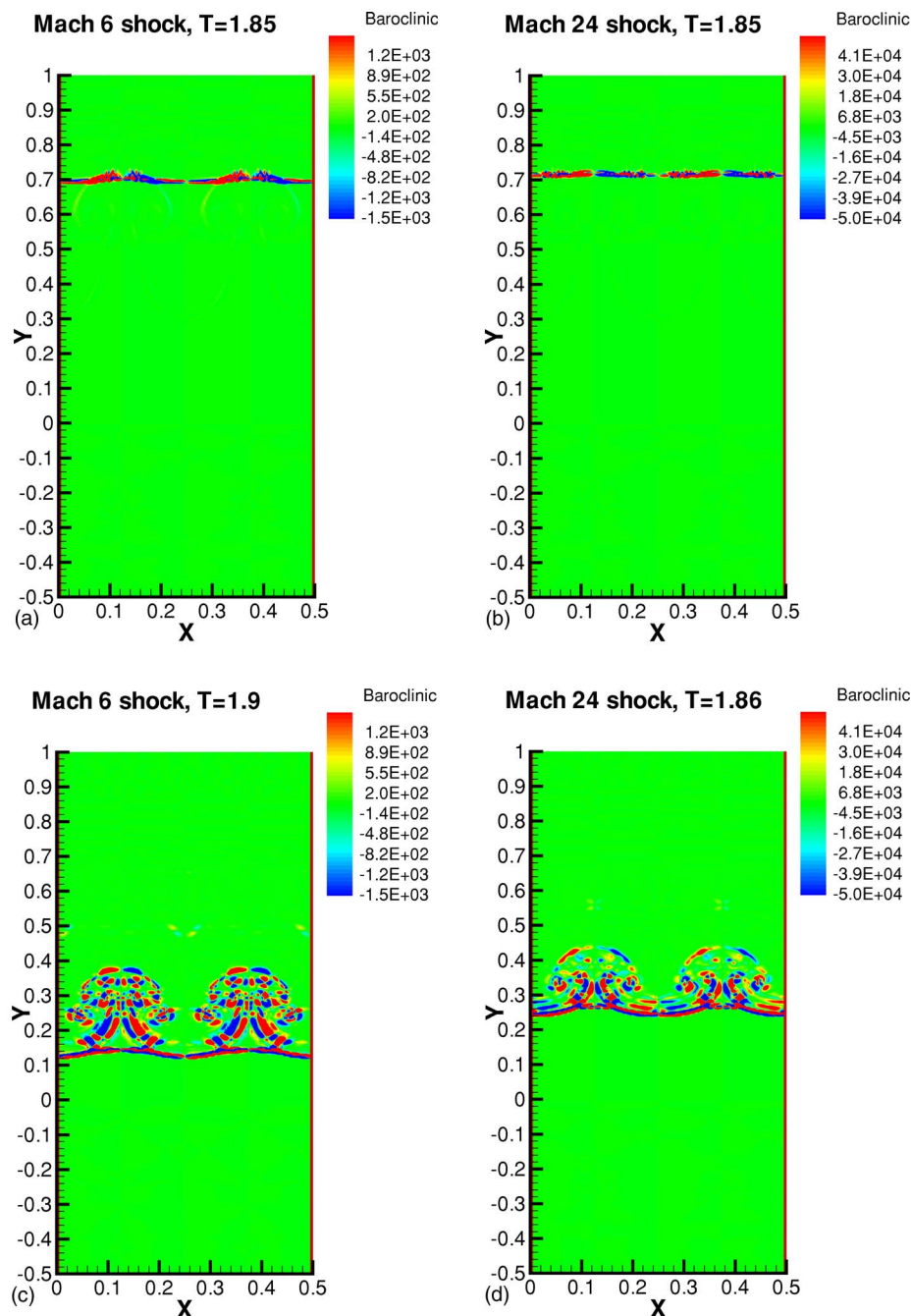


FIG. 11. (Color online) Shock interacts with Rayleigh-Taylor flows. Left: Mach 6 shock; right: Mach 24 shock. Top: shock just hits the head of the RT interface; bottom: shock just leaves the tail of the RT interface. Baroclinic vorticity source.

## V. CONCLUDING REMARKS

We observe, through a systematic numerical simulation of the two-dimensional Navier-Stokes equation, that shocks interacting with a Rayleigh-Taylor interface can speed up the transition to full instability for the Rayleigh-Taylor interface significantly. Stronger shocks are more effective in this speed-up process. This conclusion is valid regardless of whether the shock hits the head or the tail of the Rayleigh-Taylor interface.

## ACKNOWLEDGMENTS

C.-W.S. was supported by ARO Grant No. W911NF-04-1-0291, NSF Grants No. DMS-0207451 and No. DMS-0510345, and AFOSR Grant No. FA9550-05-1-0123. The

work of Y.Z. was performed under the auspices of the U.S. Department of Energy by the University of California Lawrence Livermore National Laboratory under Contract No. W-7405-Eng-48.

<sup>1</sup>L. Rayleigh, Proc. R. Math. Soc. **14**, 170 (1883).

<sup>2</sup>G. I. Taylor, Proc. R. Soc. London, Ser. A **201**, 192 (1950).

<sup>3</sup>S. Chandrasekhar, *Hydrodynamic and Hydromagnetic Stability* (Oxford University Press, Oxford, 1961).

<sup>4</sup>D. Sharp, Physica D **12**, 3 (1984).

<sup>5</sup>C. L. Gardner, J. Glimm, O. McBryan, R. Menikoff, D. H. Sharp, and Q. Zhang, Phys. Fluids **31**, 447 (1988).

<sup>6</sup>Y.-N. Young, H. Tufo, A. Dubey, and R. Rosner, J. Fluid Mech. **447**, 377 (2001).

<sup>7</sup>Y. Zhou, H. F. Robey, and A. C. Buckingham, Phys. Rev. E **67**, 056305 (2003).

<sup>8</sup>L. Smarr, J. R. Wilson, R. P. Barton, and R. L. Bowers, Astrophys. J. **246**,

- 515 (1981).
- <sup>9</sup>W. D. Arnett, J. N. Bahcall, R. T. Kirshner, and S. E. Woosley, *Annu. Rev. Astron. Astrophys.* **27**, 629 (1989).
- <sup>10</sup>J. Lindl, *Internal Confinement Fusion: The Quest for Ignition and Energy Gain* (Springer, New York, 1997).
- <sup>11</sup>Y. Zhou, B. A. Remington, H. F. Robey *et al.*, *Phys. Plasmas* **10**, 1883 (2003).
- <sup>12</sup>Y. Zhou, R. Rubinstein, D. Eliason, and W. Cabot, *Astron. Astrophys.* **405**, 379 (2003).
- <sup>13</sup>Y. Zhou, G. Zimmerman, and E. Burke, *Phys. Rev. E* **65**, 056303 (2002).
- <sup>14</sup>G. F. Carnevale, P. Orlandi, Y. Zhou, and R. C. Kloosterziel, *J. Fluid Mech.* **457**, 181 (2002).
- <sup>15</sup>G. Pacitto, C. Flament, J.-C. Bacri, and M. Widom, *Phys. Rev. E* **62**, 7941 (2000).
- <sup>16</sup>C. Mügler and S. Gauthier, *Phys. Fluids* **12**, 1783 (2000).
- <sup>17</sup>D. Balsara and C.-W. Shu, *J. Comput. Phys.* **160**, 405 (2000).
- <sup>18</sup>C.-W. Shu and S. Osher, *J. Comput. Phys.* **77**, 439 (1988).
- <sup>19</sup>G. Jiang and C.-W. Shu, *J. Comput. Phys.* **126**, 202 (1996).
- <sup>20</sup>Y.-T. Zhang, J. Shi, C.-W. Shu, and Y. Zhou, *Phys. Rev. E* **68**, 046709 (2003).
- <sup>21</sup>J. Shi, Y.-T. Zhang, and C.-W. Shu, *J. Comput. Phys.* **186**, 690 (2003).
- <sup>22</sup>T. S. Lundgren, "A free vortex method with weak viscous effects," in *Mathematic Aspects of Vortex Dynamics*, edited by R. E. Caflish (SIAM, Philadelphia, 1989).
- <sup>23</sup>J. Z. Wu, *Phys. Fluids* **7**, 2375 (1995).
- <sup>24</sup>G. Tryggvason, *J. Comput. Phys.* **75**, 253 (1988).
- <sup>25</sup>Th. von Karman, "On the foundation of high speed aerodynamics," in *General Theory of High Speed Aerodynamics*, edited by W. R. Sears (Princeton University Press, Princeton, NJ, 1954).
- <sup>26</sup>M. J. Lighthill, *J. Fluid Mech.* **2**, 1 (1956).
- <sup>27</sup>W. D. Hayes, *J. Fluid Mech.* **2**, 595 (1957).